SOLIDS
AND LIQUIDS

Vibrational Spectra and Elastic Piezoelectric and Polarization Properties of the α-SrB₄O₇ Crystal

V. I. Zinenko, M. S. Pavlovskii, A. I. Zaitzev, A. S. Krylov, and A. S. Shinkorenko

Kirensky Institute of Physics, Siberian Branch, Russian Academy of Sciences, Krasnoyarsk, 660036 Russia
e-mail: zvi@iph.krasn.ru
Received February 15, 2012

Abstract—The crystal lattice vibrational frequencies in the center of the Brillouin zone have been determined with the Raman spectroscopy method. The lattice vibrational frequencies, the phonon density of states, elastic and piezoelectric moduli, Born dynamic charges, and high-frequency dielectric constant have been calculated using the density functional method. All calculated quantities have been compared to the experimental data. A model of a nonpolar paraelectric phase for this compound, as well as a mechanism of the formation of domain in it, has been proposed. The polarization in the experimentally observed polar phase has been calculated.

DOI: 10.1134/S1063776112080195

1. INTRODUCTION

Crystals with the structure of a stable modification of strontium tetraborate α-SrB₄O₇ (SBO) are known for a long time [1, 2]. Other representatives of this structure type PbB₄O₇ and EuB₄O₇ [3], as well as a quite recently revealed high-pressure phase β-CaB₄O₇ [4], are also known. The structure of these crystals belongs to the rhombic system with the *Pnm*2₁ polar space group and has a number of structural features rare for borate compounds: their crystal structure is based on a three-dimensional network formed only from boron−oxygen tetrahedra and oxygen three-coordinated in boron is present in some structural sites [5]. For this reason, their atomic density is high for borate compounds. These structural features in SBO and PbB₄O₇ crystals are possibly manifested in high (for substances with not too high melting temperature) velocities of bulk acoustic waves [6−8].

In last decades, SBO crystals have attracted significant interest owing to their relatively high nonlinear optical coefficients, wide transparency window (up to 130 nm), and high resistance to optical damage. Owing to these properties, these crystals are very promising for nonlinear optical conversion of radiation in the far ultraviolet spectral range [7, 9, 10]. However, the birefringence of the SBO crystal is small, which complicates the achievement of angular matching for such a conversion in a single-domain sample. In the case of ferroelectric crystals, phase matching can be achieved owing to quasi-synchronism by creating a domain structure with a certain period and with the opposite direction of the polarization in domains [11]. At present, there are no experimental data confirming ferroelectric phenomena in SBO crystals. However, the SBO crystal has a unique feature, because such domain (twin) structures spontaneously appearing in these crystals in the process of their growth were revealed [12, 13]. However, these domains cannot be repolarized by really achievable electric fields. Thus, the magnitude of the polarization, as well as the mechanism of the formation of domains in SBO crystals, remains unknown.

A fairly large amount of information on the elastic, piezoelectric, and vibrational properties of the crystals of this family has been already collected [6−14], but this information for the SBO crystal is insufficiently complete. In particular, the elastic constants of this crystal were measured in [8] and the experimental values of some piezoelectric constants were presented in [7]. Information on the vibrational spectra of the SBO crystal is apparently absent.

The aim of this work is to experimentally determine the limiting vibrational frequencies and to theoretically calculate the dynamics of the crystal lattice, elastic and piezoelectric constants, and magnitude of the polarization of the SBO crystal.

2. RAMAN SPECTRA

The SrB₄O₇ crystal was grown by the Czochralski method from a melt with the stoichiometric ratio; the details of the growth process can be found in [12].

The experimental cell parameters and coordinates of ions [2] are summarized in Table 1 (the first row for each ion). The unit cell contains two molecular units. The structure of the crystal is shown in Fig. 1.

The polarization Raman spectra were performed at room temperature (295 K) with a Horiba Jobin Yvon T64000 spectrometer in the 90° scattering geometry. The spectrometer operated in the dispersion subtraction mode with an input-slit spectral resolution of 2 cm⁻¹. An Ar⁺ laser (a wavelength of λ = 514 nm) was

Table 1. Lattice parameters and relative coordinates of the atoms of the SBO crystal in the rhombic polar phase

$Pnm2_1$			$a = 4.4145$ Å	$b = 10.6827$ Å	$c = 4.2234$ Å
	Wikoff position		x	y	z
Sr	2a	exp.	0.71205		0.07090
		calc.	0.66820	0	0.00760
		ideal.	0.66666		0.16666
B(1)	4b	exp.	0.32256	0.24907	0.06532
		calc.	0.32800	0.24930	0.05848
		ideal.	0.33333	0.25000	0.04166
B(2)	4b	exp.	0.17443	0.12193	0.53942
		calc.	0.17510	0.11990	0.54860
		ideal.	0.16666	0.12500	0.54166
O(1)	4b	exp.	0.85540	0.14109	0.61244
		calc.	0.87080	0.15270	0.58960
		ideal.	0.83333	0.12500	0.66666
O(2)	4b	exp.	0.63322	0.27714	0.20812
		calc.	0.61710	0.29010	0.23050
		ideal.	0.66666	0.25000	0.16666
O(3)	2a	exp.	0.27481		0.64664
		calc.	0.23660	0	0.64180
		ideal.	0.33333		0.66666
O(4)	4b	exp.	0.22508	0.13528	0.20324
		calc.	0.26150	0.14440	0.23540
		ideal.	0.16666	0.12500	0.16666

used to excite the scattering spectrum. The radiation power on the sample was 80 mW, which corresponds to a laser radiation density of 250 W/cm². We use the standard notation [15] to describe the geometry of Raman scattering. The decomposition of the vibrational representation into irreducible representation in the center of the Brillouin zone has the form

$$\Gamma = 19A_1 + 17A_2 + 17B_1 + 19B_2.$$
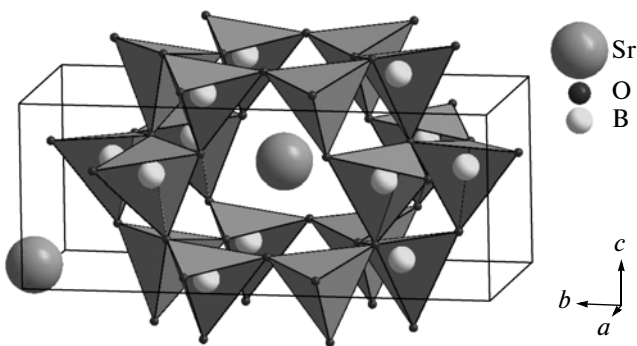
Fig. 1. Structure of the SrB_4O_7 crystal in the rhombic phase with the $Pnm2_1$ space group.

Optical modes A_1, B_1, and B_2 are polar and active in both Raman and infrared spectra. Nonpolar modes A_2 are only Raman active. Figure 2 shows the vibrational spectrum in various scattering geometries. Table 2 presents the measured vibrational frequencies.

3. DYNAMICS OF THE CRYSTAL LATTICE

The lattice dynamics, high-frequency dielectric constant, Born dynamic charges, and elastic and piezoelectric properties were calculated within a non-empirical ionic-crystal model including the dipole and quadrupole polarizabilities of ions. The details of the model were given in [16]. All calculations were performed for the experimental lattice parameters. Some vibrational frequencies calculated with the experimental coordinates of ions (see Table 1) were imaginary. To eliminate these unstable vibrational modes, we used the coordinates of the ions in the unit cell slightly different from the experimental values. These coordinates are presented in Table 1 (second row for each ion), where it can be seen that these changes in the coordinates of the ions are insignificant. The calculated frequencies in the center of the Brillouin zone are given in Table 2. According to Table 2, some calcu-

lated frequencies in the range from 200 to 800 cm^{-1} are in satisfactory agreement with the experimental values, whereas discrepancy between the calculated and experimental values in the range of 500–600 cm^{-1} reaches about 30%. The frequencies below 100 cm^{-1} and above 1000 cm^{-1}, as well as some frequencies inside this range, are not observed experimentally. Figure 3 shows the phonon densities of states in the entire Brillouin zone and partial densities of states of each ion. The following feature of the calculated density of states is noteworthy: as can be seen in Fig. 3, in the low-frequency range below 100 cm^{-1}, strontium ions are predominantly displaced in the vibrational eigenvectors, whereas the displacements of oxygen and boron ions are negligibly small compared to the displacements of strontium ions. The situation in the vibrational spectrum above 100 cm^{-1} is inverse.

Table 3 summarizes the calculated components of the tensor of Born dynamic charges. The calculated elastic constants and dielectric constant are given in Table 4 in comparison with the experimental data [7, 8]. According to this table, agreement between the calculated and experimental elastic properties of the SBO crystal is satisfactory except for the shear elastic constants C_{12}, C_{13}, and C_{23}, for which the calculated and experimental values differ by a factor of 2. The calculated piezoelectric constants are $e_{15} = 0.71$ C/m^2, $e_{24} = 0.22$ C/m^2, $e_{31} = 1.23$ C/m^2, $e_{32} = 1.03$ C/m^2, and $e_{33} = 1.93$ C/m^2. Table 4 presents the piezoelectric
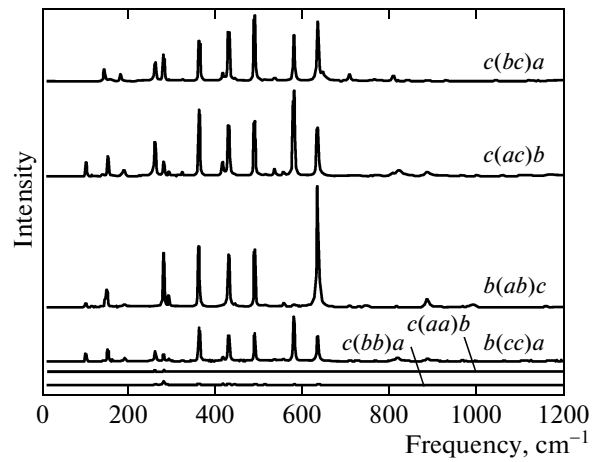

Fig. 2. Raman spectra of the SrB$_4$O$_7$ crystal in the rhombic phase.

moduli $d_{lk} = e_{li}(C_{ik})^{-1}$ in comparison with the existing experimental values [7].

4. SPONTANEOUS POLARIZATION

The structure of the SBO crystal includes a framework of oxygen tetrahedra with a boron ion in each of them that are connected with each other through vertices. This framework contains quite large cavities with strontium ions (Fig. 1).

Table 2. Extreme vibrational frequencies (in inverse centimeters) of the SBO crystal in the rhombic polar phase

| A_1			A_2		B_1		B_2	
exp.		calc.	exp.	calc.	exp.	calc.	exp.	calc.
TO	LO							
102	146	13	102	90	262	46	263	53
150	182	62	153	120	280	130	281	72
191	260	204	192	203	364	231	363	201
281	282	240	262	240	431	263	416	212
292	360	253	280	312	442	367	439	252
361	416	322	294	341	491	392	491	329
430	433	349	325	381	514	435	535	349
490	490	397	362	413	581	477	555	381
633	580	421	431	441	635	502	582	433
707	632	442	490	479		610	633	502
750	708	455	580	544		733	726	587
815	808	533	634	554		766	818	645
886		553	819	762		791		703
988		734	886	794		901		835
		765		969		978		960
		962		982		1090		975
		975		1119				1051
		1073						1107
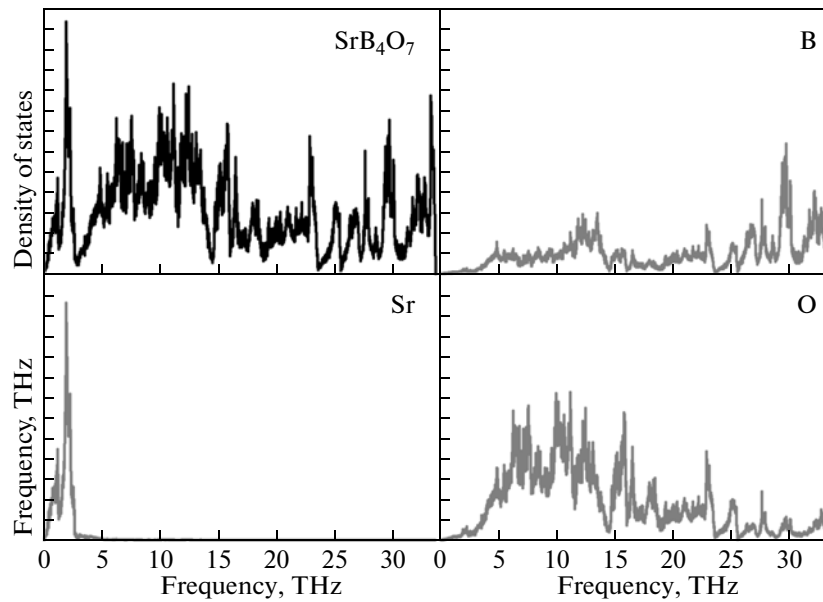
Fig. 3. Calculated total and partial phonon densities of states of the SBO crystal.

To calculate the polarization in strontium tetraborate, we assume that this crystal has a paraelectric phase with a higher symmetry although such a phase has not yet been observed experimentally in this compound and compounds isostructural to it. The struc-

Table 3. Components of the tensor of dynamic Born charges of the SBO crystal in the polar phase in the units of the elementary charge

		Z_x	Z_y	Z_z
	Z_x	2.87	0.00	−0.04
Sr	Z_y	0.00	3.17	0.00
	Z_z	−0.05	0.00	2.63
	Z_x	3.03	−0.85	−0.27
B_1	Z_y	−0.11	2.68	0.25
	Z_z	0.23	−0.56	4.22
	Z_x	3.81	0.24	−0.16
B_2	Z_y	−0.59	3.74	−1.08
	Z_z	0.05	0.20	3.31
	Z_x	−3.68	1.78	−0.04
O_1	Z_y	1.74	−2.09	0.26
	Z_z	0.49	−0.06	−1.07
	Z_x	−2.40	−0.74	−0.79
O_2	Z_y	−1.05	−1.28	0.82
	Z_z	−0.40	1.00	−3.60
	Z_x	−1.36	0.00	−0.24
O_3	Z_y	0.00	−4.89	0.00
	Z_z	−0.27	0.00	−1.21
	Z_x	−1.51	−0.63	1.09
O_4	Z_y	−0.51	−2.20	1.53
	Z_z	0.81	1.64	−3.59

ture of the paraelectric phase is as follows. As was mentioned above, the structure of strontium tetraborate is based on the framework of boron–oxygen tetrahedra. All these tetrahedra are distorted, but they can be made regular by quite slightly displacing oxygen atoms, as can be seen in Fig. 1. In this case, the lattice parameters are expressed in terms of the length of the edge of this regular tetrahedron as

$$\mathbf{a} = \mathbf{r}\sqrt{3}, \quad \mathbf{b} = 4\mathbf{r}, \quad \mathbf{c} = \mathbf{r}\sqrt{8/3}.$$

Expressing the lattice parameters in terms of the length of the edge of this regular oxygen tetrahedron and making the necessary displacement of oxygen atoms, we obtain the regular structure framework with new regular cavities. A strontium ion is placed in the center of each such cavity and a boron ion is placed inside each tetrahedron. Thus, we obtain an idealized structure in the polar phase with the same $Pnm2_1$ symmetry space group and also with two molecules in the unit cell. The coordinates of the ions in this idealized structure are presented in Table 1 (third row for each ion). According to this table, the maximum displacements of the ions necessary for obtaining such an ideal structure are no more than 1 Å.

An important feature of this structure (see Fig. 4a) is that each tetrahedron in it can be completed to a triangular bipyramid consisting of two regular tetrahedra, which are connected with each other by the edge perpendicular to the c axis of the crystal and one of the tetrahedra contains the boron ion, whereas the other does not contain it. It can be clearly seen that this ideal structure is really based on the framework consisting not of tetrahedra, but of bipyramids connecting with each other through edges. The unit cell of the crystal contains eight bipyramids. If each boron ion is dis-

Table 4. Elastic moduli C_{ij}, piezoelectric moduli d_{ij}, and high-frequency dielectric constant ε_{ii} of the SBO crystal in the rhombic polar phase

C_{ij}, GPa, calc.	C_{ij}, GPa, exp. [8]	d_{ij}, pm/V, ε_{ii}, calc.	d_{ij}, pm/V, ε_{ii}, exp. [7]
$C_{11} = 318$	$C_{11} = 304 \pm 4$	$\varepsilon_{xx} = 4.38$	$\varepsilon_{xx} = 3.01$
$C_{12} = 132$	$C_{12} = 70 \pm 35$	$\varepsilon_{yy} = 4.28$	$\varepsilon_{yy} = 2.97$
$C_{13} = 90$	$C_{13} = 49 \pm 29$	$\varepsilon_{yy} = 4.66$	$\varepsilon_{yy} = 3.03$
$C_{22} = 370$	$C_{22} = 268 \pm 1$	$d_{15} = 8.16$	–
$C_{23} = 114$	$C_{23} = 55 \pm 33$	$d_{24} = 2.08$	–
$C_{33} = 355$	$C_{33} = 378 \pm 3$	$d_{31} = 2.33$	$d_{31} = 1.31$
$C_{44} = 106$	$C_{44} = 139 \pm 2$	$d_{32} = 0.51$	$d_{32} = 1.62$
$C_{55} = 87$	$C_{55} = 120 \pm 4$	$d_{33} = 4.68$	
$C_{66} = 124$	$C_{66} = 133 \pm 2$		

Table 5. Energy and contributions to it for the experimental and ideal structures of the SBO crystal with the subtracted energy and the corresponding contributions for the disordered paraelectric phase

	E_{tot}, eV	E_{Coul}, eV	E_{shot}, eV	E_{dip}, eV	E_{qd}, eV
E_{exp}, eV	−6.81	−32.92	16.30	10.62	−0.46
E_{ideal}, eV	−1.86	−3.48	−0.40	2.02	−0.06

placed from the tetrahedron where it is located in the bipyramid to the other tetrahedron in the same bipyramid, neither translational nor point symmetry of the ideal structure is changed; only the direction of the polarization of the crystal is changed to opposite.

Thus, in view of the above discussion, it is reasonable to assume that the paraelectric phase of strontium tetraborate is a structure in which boron ions in each bipyramid equiprobably occupy the positions inside its regular tetrahedra (Fig. 4b). In this case, the coordinates of oxygen and strontium ions correspond, as before, to "ideal" values presented in the third row of Table 1. Such a structure belongs to the nonpolar rhombic space group *Pnmm* with two molecules in the ideal crystal; i.e., the disordering of boron ions in two positions does not change the translational symmetry of the crystal.

To estimate the depth of the minimum, the position of the boron ion inside the tetrahedron, and the energy barrier between two equiprobable positions of boron in the bipyramid, we calculated the total energy of the ideal structure as a function of the displacement of the boron ion along the *c* axis of the crystal (i.e., along the line connecting the opposite vertices of the bipyramid) from one tetrahedron to the other. In this case, the strontium and oxygen ions remained in the ideal positions. This total energy for various volumes of the unit cell is shown in Fig. 5, where it can be seen that the minimum energy at the equilibrium volume corresponds to the boron position displaced from the center of the tetrahedron toward its base; in this case, the energy barrier between two boron positions in the

bipyramid is 0.22 eV. When the volume of the cell decreases (increases), which corresponds to the application of the positive (negative) hydrostatic pressure, the minimum energy corresponds to the larger (smaller) displacement of boron from the center of the tetrahedron and the energy barrier between two boron positions in the bipyramid increases (decreases).

It is noteworthy that, when the symmetry of the ideal crystal is reduced owing, e.g., to the displacement of strontium ions from the center of the cavity, the symmetric potential with two minima for the boron ion naturally becomes asymmetric and the depth of the minimum depends strongly on the displacement of strontium, as is illustrated in Fig. 6.

We now discuss the energy properties of ideal disordered, ordered, and experimentally observed struc-
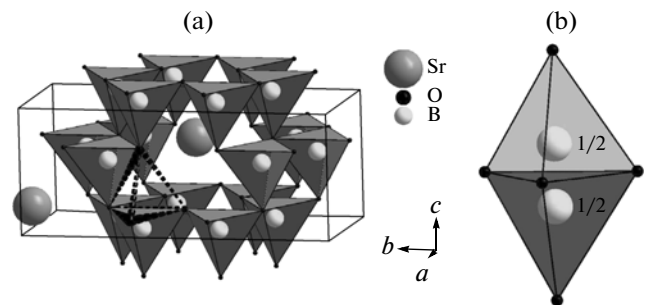
Fig. 4. (a) Idealized structure of the SBO crystal in the $Pnm2_1$ polar phase, the dotted tetrahedron is an empty tetrahedron in a bipyramid and (b) two positions of the boron ion in the *Pnmm* nonpolar phase.
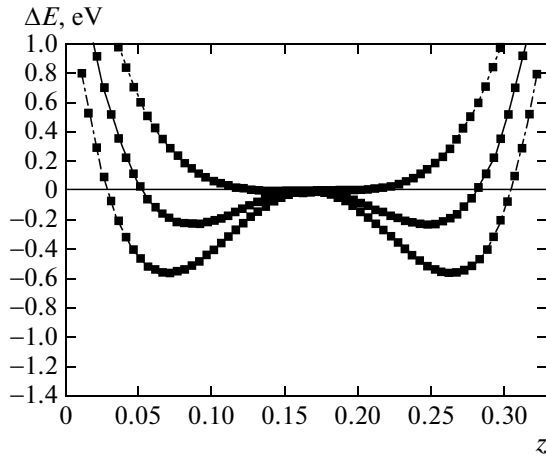
Fig. 5. Change $\Delta E = E - E_0$ in the total energy of the SBO crystal measured from the energy E_0 of the crystal where boron ions are placed in the centers of bipyramid versus the relative displacement of boron ions parallel to the polar axis at equilibrium volumes of the unit cell of (solid curve) 92.6, (dashed curve) 101.6, and (dash–dotted curve) 86.9 Å^3.
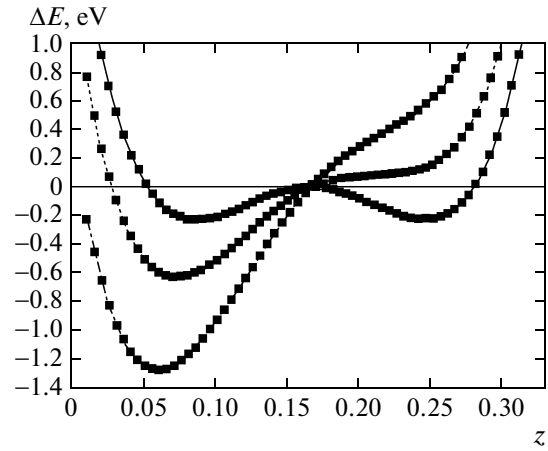
Fig. 6. Change $\Delta E = E - E_0$ in the total energy of the SBO crystal measured from the energy E_0 of the crystal where boron ions are placed in the centers of bipyramid versus the relative displacement of boron ions parallel to the polar axis at a displacement of (solid curve) 0, (dashed curve) 0.12, and (dash–dotted curve) 0.29 Å of the strontium ions from the ideal positions in the structure with the *Pnmm* symmetry.

tures. The total energy of the ideal crystal in which the boron ion equiprobably occupies two equilibrium positions in the bipyramid is approximately estimated as follows. As was mentioned above, the unit cell of the crystal contains eight regular bipyramids; in each of these bipyramids, boron is located inside in one of two tetrahedra. Then, the energy E_{av} of the disordered *Pnmm* phase can be evaluated by averaging the calculated energies of the structures of $2^8 = 256$ configurations. The corresponding value is $E_{av} = -404.79$ eV (disregarding the self-energy of the ions) and consists of the following contributions: the Madelung energy $E_{av}^{Coul} = -463.38$ eV, the short-range interaction energy $E_{sv}^{sh} = 74.8$ eV, the dipole energy $E_{av}^{dip} = -15.65$ eV, and the quadrupole energy $E_{av}^{qd} = 0.76$ eV. Table 5 presents the differences between the energies, as well as individual contributions to these differences, of the nonpolar disordered phase and polar ordered ideal and experimentally observed phases. As can be seen in this table, the energy differences are negative and large in absolute value, and the main contribution to these differences comes from the Madelung energy. Thus, the results of this calculation shows that the temperature of the phase transition from the polar ordered phase to a hypothetical nonpolar disordered phase should be

very high, much higher than the melting temperature $T_{melt} = 1273$ K of the SBO crystal.

The existence of the BaB$_4$O$_7$ crystal in the β phase with the nonpolar symmetry space group *Pmnb* and four molecules in the unit cell [17] can be an additional reason in favor of the proposed model of the paraelectric phase. The cell parameter **a** in the BaB$_4$O$_7$ structure is twice as large as this parameter in the SrB$_4$O$_7$ structure, the parameters **b** and **c** in both structures are fairly close, boron ions in one half of this doubled cell in BaB$_4$O$_7$ occupy the same positions in the bipyramids as in SrB$_4$O$_7$ (lower part of the bipyramid in Fig. 4b), and boron ions in the other half occupy the opposite positions in the bipyramids (upper part of Fig. 4b). Thus, in terms of the model of the disordering of boron ions in the compounds under consideration, "antiferroelectric" ordering occurs in the experimentally observed BaB$_4$O$_7$ structure. It is noteworthy that the calculation performed in this work shows that the energies of the structures with the ferroelectric and antiferroelectric types of ordering of boron ions and with subsequent displacements of oxygen ions and cations are close for SrB$_4$O$_7$, CaB$_4$O$_7$, PbB$_4$O$_7$, and BaB$_4$O$_7$ compounds (isomorphic under the assumption of the paraelectric phase with the *Pnmm* symmetry), as can be seen in Table 6. This closeness of the energies of the ferroelectric and antiferroelectric states can also indicate that it was reasonable to assume that these compounds have a paraelectric phase. It follows from Table 6 that a polar state is implemented in SrB$_4$O$_7$, CaB$_4$O$_7$, and PbB$_4$O$_7$, whereas the antipolar state occurs for the BaB$_4$O$_7$ compound in complete agreement with the experimental situation [2–4, 17].

Table 6. Differences ΔE of the total energies of the phases with the structures α-SrB$_4$O$_7$ and β-BaB$_4$O$_7$ for various borate crystals

	SrB$_4$O$_7$	CaB$_4$O$_7$	PbB$_4$O$_7$	BaB$_4$O$_7$
ΔE, eV	−0.04352	−0.16864	−0.01360	0.25840

The spontaneous polarization per unit volume of the unit cell in the observed polar phase within the model under consideration can be calculated as the sum of three terms:

$$P = P_{dip} + P_{ion} + P_{el} = 114 \ \mu C/cm^2.$$

Here $P_{dip} = 41 \ \mu C/cm^2$ is the sum of the dipole moments associated with the ordering of boron ions inside of one of the tetrahedra of the bipyramid (the disordering of boron ions in two equivalent positions in the bipyramid can be treated as the disordered of the dipole moment of the bipyramid $B^{3+}O_5^{0.6-}$ in two states, see Fig. 4b), $P_{ion} = 69 \ \mu C/cm^2$ is the polarization calculated as the sum of the products of the nominal charges of ions by their displacements under the distortion of the ideal polar structure to the experimentally observed structure, and $P_{el} = 4 \ \mu C/cm^2$ is the polarization owing to the dipole distortions of the electron density of ions.

5. CONCLUSIONS

The limiting vibrational frequencies of the crystal lattice of the α-SrB_4O_7 crystal have been measured with the Raman spectroscopy method.

The total vibrational spectrum of the crystal lattice, elastic and piezoelectric constants, Born dynamic charges, and high-frequency dielectric constant have been calculated within the nonempirical ionic-crystal model. The calculated properties of the SBO crystal are in satisfactory agreement with the experimental data. The performed calculation reproduces large longitudinal components of the experimentally observed elastic constants. The existing discrepancy between the calculated and measured values of some shear components of the elastic constants and piezoelectric moduli can be attributed both to the roughness of the used ionic-crystal model in application to compounds with a boron atom and to the inaccuracy of the experimental determination of these quantities (shear elastic moduli and piezoelectric constants for low-symmetry structures are determined with large errors). To explain the experimentally observed domain structure in the SBO crystal appearing in the process of growth, we have proposed the model of a hypothetical centrosymmetric paraelectric phase with the *Pnmm* symmetry space group in which boron ions are disordered in tow equiprobable equilibrium positions in the BO_5 regular bipyramid. Comparison of the energies of the crystal calculated for the ordered ideal and experimentally observed structures with an estimate of the energy of the crystal in the paraelectric phase shows that the differences of the energies of the ordered phases (ideal and experimental) from the energy of the paraelectric phase are several ten thousands degrees, which is much higher than the melting temperature of the SBO crystal and, therefore, the phase transition from the polar *Pnm*2$_1$ phase to the nonpolar *Pnmm*

phase cannot be observed. The assumption of the hypothetical nonpolar paraelectric phase allowed the calculation of the spontaneous polarization in the experimentally observed structure; this spontaneous polarization is about 114 $\mu C/cm^2$, which is several times larger than the polarization in the classical ferroelectric compound $BaTiO_3$.

REFERENCES

1. J. Krogh-Moe, Acta Chem. Scand. **18**, 2055 (1964).
2. S. Block, A. Perloff, and C. E. Weir, Acta Crystallogr. **17**, 314 (1964).
3. K. Machida, H. Hata, K. Okuno, G. Adachi, and J. Shiokawa, J. Inorg. Nucl. Chem. **41**, 1425 (1979).
4. H. Huppertz, Z. Naturforsch., B: Anorg. Chem., Org. Chem. **58b**, 257 (2003).
5. F. Pan, G. Shen, R. Wang, X. Wang, and D. Shen, J. Cryst. Growth **241**, 108 (2002).
6. K. S. Aleksandrov, A. V. Zamkov, A. I. Zaitsev, P. P. Turchin, A. M. Sysoev, and A. A. Parfenov, Phys. Solid State **46** (9), 1636 (2004).
7. A. I. Zaitsev, A. S. Aleksandrovskii, A. V. Zamkov, and A. M. Sysoev, Inorg. Mater. **42** (12), 1360 (2006).
8. I. Martynyuk-Lototska, T. Dudok, O. Mys, and R. Vlokh, Opt. Mater. **31**, 660 (2009).
9. S. Yu. Oseledchik, A. L. Prosvirnin, A. I. Pisarevskiy, V. V. Starshenko, V. V. Osadchuk, S. P. Belokrys, N. V. Svitanko, A. S. Korol, S. A. Krikunov, and A. F. Selevich, Opt. Mater. **4**, 669 (1995).
10. V. Petrov, F. Noack, D. Shen, F. Pan, G. Shen, X. Wang, R. Komatsu, and V. Alex, Opt. Lett. **29**, 373 (2004).
11. V. G. Dmitriev and L. V. Tarasov, *Applied Nonlinear Optics* (Fizmatlit, Moscow, 2004) [in Russian].
12. A. I. Zaitsev, A. S. Aleksandrovsky, A. D. Vasiliev, and A. V. Zamkov, J. Crystal Growth **310**, 1 (2008).
13. A. S. Aleksandrovsky, A. M. Vyunyshev, and A. I. Zaitsev, in *Handbook on Borates: Chemistry, Production, and Applications*, Ed. by M. P. Chung (Nova Science, New York, 2010), Chap. 5, p. 159.
14. Y. Wang, M. Feng, H. Wang, P. Fu, J. Wang, X. Cao, and G. Lan, J. Phys.: Condens. Matter **19**, 436207 (2007).
15. D. L. Rousseau, R. P. Bauman, and S. P. S. Porto, J. Raman Spectrosc. **10**, 253 (1981).
16. E. G. Maksimov, V. I. Zinenko, and N. G. Zamkova, Phys.—Usp. **47** (11), 1075 (2004).
17. J. S. Knyrim, S. R. Römer, W. Schnick, and H. Huppertz, Solid State Sci. **11**, 336 (2009).

Translated by R. Tyapaev